ADVANCED FUNCTIONAL MATERIALS
www.afm-journal.de

FULL PAPER

Biologically Enabled Syntheses of Freestanding Metallic Structures Possessing Subwavelength Pore Arrays for Extraordinary (Surface Plasmon-Mediated) Infrared Transmission

Yunnan Fang, Vincent W. Chen, Ye Cai, John D. Berrigan, Seth R. Marder, Joseph W. Perry, and Kenneth H. Sandhage**

A scalable wet chemical process has been used to convert the intricate silica microshells (frustules) of diatoms into gold structures that retained the three-dimensional (3-D) frustule shapes and fine patterned features. Combined use of an amine-enriching surface functionalization protocol and electroless deposition yielded thin (<100 nm) conformal nanocrystalline gold coatings that, upon selective silica dissolution, were converted into freestanding gold structures with frustule-derived 3-D morphologies. By selecting a diatom frustule template with a quasi-regular hexagonal pore pattern (*Coscinodiscus asteromphalus, CA*), gold replica structures possessing such pore patterns were produced that exhibited infrared transmission maxima/reflection minima that were not observed for the starting silica diatom frustules or for flat nonporous gold films; that is, such extraordinary optical transmission (EOT) resulted from the combined effects of the quasi-periodic hexagonal hole structure (inherited from the *CA* diatom frustules) and the gold chemistry. Calculated and measured IR transmission spectra obtained from planar gold films with quasi-periodic hexagonal *CA*-derived hole patterns, or with short-range periodic hexagonal hole patterns, indicated that the enhanced IR transmission exhibited by the gold *CA* frustule replicas was enabled by the generation and transmission of surface plasmons. This scalable bio-enabled process provides a new and attractive capability for fabricating self-supporting, responsive, 3-D metallic structures for use as dispersible/harvestable microparticles tailored for EOT-based applications.

1. Introduction

Nature provides impressive examples of organisms capable of forming organic and inorganic structures with intricate and controlled three-dimensional (3-D) hierarchical (nanoscale-to-macroscale) morphologies.[1] Among the most versatile of structure-forming organisms are diatoms, a type of aquatic single-celled algae.[2] Each diatom species forms a silica-bearing microshell (frustule) with a particular 3-D shape and with specific patterns of fine features (pores, ridges, channels, protuberances, etc.).[2] Owing to the species-specific nature of diatom silica structure formation, a rich variety of 3-D silica morphologies can be found among the estimated 10^4–10^5 extant diatom species.[2] The sustained reproduction (repeated doubling) of a given species of diatom can yield enormous numbers of daughter diatoms with similarly-shaped frustules (e.g., 80 reproduction cycles corresponds to $2^{80} \approx 1.2 \times 10^{24}$ – twice Avogadro's number of frustule copies). Such massively-parallel, direct, and precise (genetically-controlled) self-assembly of structures with a wide selection of 3-D nano-to-microscale morphologies has no analogue among synthetic self-assembly processes.[3] Furthermore, the silica-based composition of diatom frustules can be altered via several shape-preserving approaches (e.g., by gas/silica displacement reactions,[4] conformal coating,[5] or combined coating and reaction methods[6]) to allow for a broader range of applications.

Certain centric diatom frustules possess organized distributions of 10^2–10^3 nm diameter pores, which has led to interest in the optical properties of these structures.[7] For example, the valves of *Coscinodiscus wailesii* diatoms have been found to exhibit wavelength selective optical transmission and optical diffraction, which have been attributed to a quasi-regular hexagonal pattern of pores on these valves.[7a] This quasi-regular pore array has also enabled *C. wailesii* valves to act as micro-lenses;

Dr. Y. Fang, Dr. Y. Cai, J. D. Berrigan, Prof. K. H. Sandhage
School of Materials Science and Engineering
Georgia Institute of Technology
771 Ferst Drive, Atlanta, GA 30332, USA
E-mail: ken.sandhage@mse.gatech.edu
V. W. Chen, Prof. J. W. Perry
School of Chemistry and Biochemistry
Georgia Institute of Technology
901 Atlantic Drive, Atlanta, GA 30332, USA
E-mail: joe.perry@gatech.edu
Prof. S. R. Marder
School of Chemistry and Biochemistry
Georgia Institute of Technology
901 Atlantic Drive, Atlanta, GA 30332, USA

DOI: 10.1002/adfm.201102715

that is, red laser light of 100 μm diameter transmitted through these valves could be focused to a diameter of <10 μm.[7b,c] The girdle bands of *C. granii* diatoms, which possess a square array of pores, have been reported to guide blue-green light.[7d] The hexagonal pore pattern on *Melosira varians* frustules has been correlated to relatively strong apparent absorption of blue light by these frustules.[7e]

In this paper, we have developed a highly-conformal, scalable, wet chemical coating process that allows the quasi-periodic pore arrays and 3-D morphologies of *Coscinodiscus asteromphalus* diatom frustules to be replicated in freestanding (silica-free) nanocrystalline gold structures. A novel and significant aspect of this wet chemical coating process is the use of a surface functionalization protocol for introducing and then amplifying (via a dendritic layer-by-layer process) amines on diatom frustule surfaces, to allow for a high degree of loading of gold(III) complexes onto such surfaces. Reduction of these complexes provides a high density of gold nanoparticles that act as preferred sites for further gold nucleation and growth, and rapid interconnection of gold nanoparticles, during exposure to an electroless plating solution. The highly-conformal and interconnected nature of the resulting thin (<100 nm) gold coatings enables the 3-D morphologies and fine patterned features of the starting diatom frustules to be well preserved upon selective silica dissolution. Consequently, we demonstrate herein for the first time that *C. asteromphalus* diatom frustules with quasi-periodic subwavelength pore arrays can be converted into freestanding nanocrystalline gold structures exhibiting extraordinary (surface plasmon-mediated) infrared transmission. Such enhanced IR transmission is a result of both the diatom-generated pore pattern and the gold chemistry of the replicas.

2. Results and Discussion

2.1. Conformal Gold Coatings

In order to coat 3-D diatom frustules with thin, conformal, continuous, and nanocrystalline gold films via electroless deposition, the relatively inert and non-conductive silica surfaces of these structures needed to be modified. Two surface functionalization approaches were examined. For the first approach, pendant amino groups were introduced to the frustule surfaces via an aminosilanization treatment. Subsequent exposure of these surface amines to a chloroauric acid solution was used to bind Au(III) complexes to the frustules. The surface-bound gold complexes were then reduced into elemental gold via reaction with sodium borohydride. The resulting gold nanoparticles were then utilized as preferred heterogeneous nucleation sites upon exposure to a commercial electroless gold deposition solution. For the second approach, a dendritic layer-by-layer process, involving sequential exposure to dipentaerythritol penta-/hexaacrylate and tris(2-aminoethyl)amine,[9] was introduced after the aminosilanization treatment, in order to significantly enrich the amine concentration on the diatom silica surfaces, while keeping all other steps the same as for the first approach. Secondary electron (SE) images of *Aulacoseira sp.* diatom frustules before and after such surface functionalization and electroless gold deposition are shown in **Figure 1**. (Note: *Aulacoseira sp.* frustules, available in large quantities as diatomaceous earth, were used to establish the desired functionalization and electroless

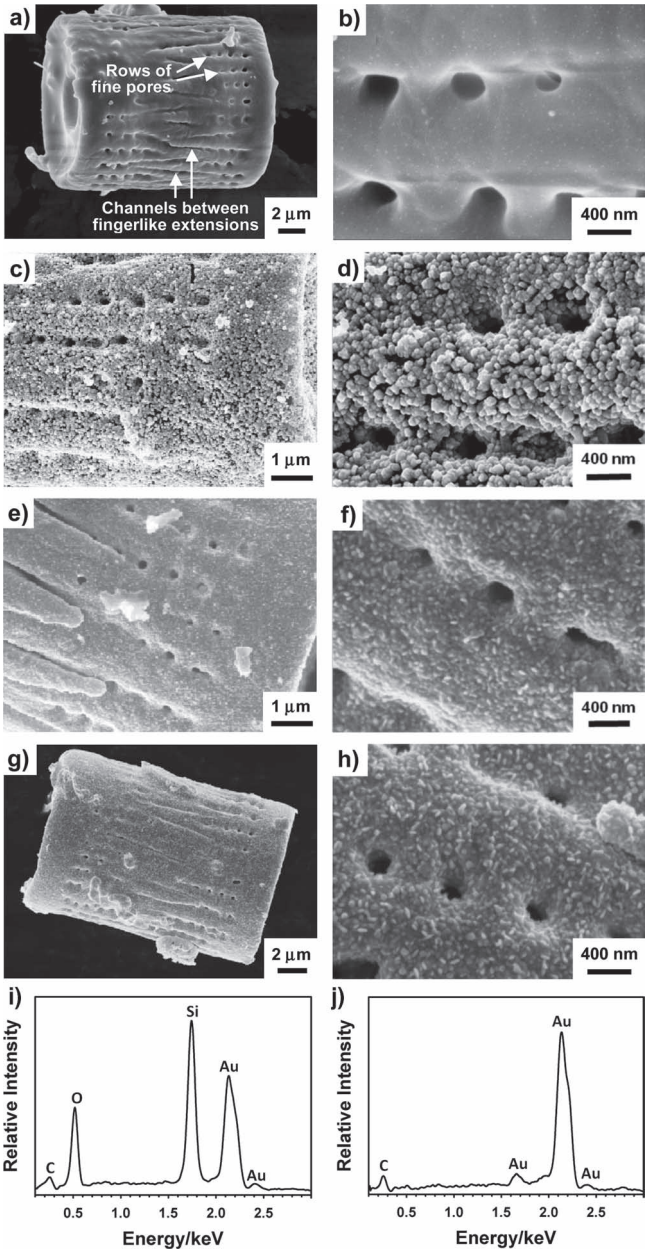

Figure 1. Secondary electron (SE) images of: a,b) a starting *Aulacoseira sp.* diatom frustule, c,d) a gold-coated *Aulacoseira sp.* diatom frustule prepared with the use of a surface functionalization treatment (involving aminosilanization) followed by electroless gold deposition, e,f) a gold-coated *Aulacoseira sp.* diatom frustule prepared with the use of an amine-amplifying surface functionalization protocol (involving aminosilanization and polyacrylate/polyamine dendritic amine amplification), followed by electroless gold deposition, g), h) a freestanding (silica-free) gold structure retaining the overall 3-D morphology of an *Aulacoseira sp.* diatom frustule prepared via selective dissolution of the silica from a gold-coated frustule of the type shown in e) and f). EDX analyses of: i) the gold-coated silica frustule shown in e) and f), and j) the freestanding gold structure shown in g) and h).

deposition protocols before application of these methods to the cultured *C. asteromphalus* diatom frustules.) These frustules possessed a cylindrical shape and contained rows of fine pores and narrow channels between intercalating fingerlike extensions (Figure 1a and b). Gold-coated surfaces of frustules that had been treated according to the first surface functionalization protocol are shown in Figure 1c and d, whereas gold-coated frustule surfaces that had been exposed to the second functionalization approach (involving dendritic amine amplification) are shown in Figure 1e and f. The gold coating prepared without use of the dendritic amine amplification treatment consisted of relatively coarse agglomerates of particles that did not conform particularly well to frustule surfaces (Figure 1c and d). Noticeable gaps were also observed in the gold coating. The aminosilanization process alone appeared to yield a modest density of surface-bound amine groups onto which a correspondingly modest concentration of surface-bound gold(III) complexes could bind. Reduction of these complexes then yielded relatively few dispersed gold particles that grew, upon subsequent electroless deposition, into relatively coarse particle agglomerates that impinged with reduced interconnectivity on frustule surfaces (Figure 1c, d). However, the gold coating formed on frustules that had been treated with the dendritic amine amplification process possessed significantly improved conformality and continuity (Figure 1e, f). The surfaces of these latter coated frustules also exhibited a finer granular appearance than for the coated frustules that had not been exposed to the amine amplification process. The enhanced population of gold(III) complexes that could bind to the amine-enriched frustule surfaces enabled the formation of a relatively high density of gold nanoparticles that could then grow and quickly impinge during subsequent electroless deposition, so as to yield a conformal and continuous coating (Figure 1e, f). To produce freestanding gold structures, the underlying silica within these coated frustules was selectively removed by dissolution in a HF solution. SE images of the resulting all-gold structures are shown in Figure 1g and h. Energy dispersive X-ray (EDX) analyses before and after exposure to the HF solution (Figure 1i and j, respectively) confirmed the selective dissolution of the underlying silica. (Note: while obvious cracks or gaps were not detected in SE images of gold-coated frustules of the type shown in Figure 1e and f, complete removal of the underlying silica by acid dissolution indicated that the gold coating was not hermetic.) Owing to the conformality and continuity of the gold coating, the freestanding (SiO_2-free) gold structures retained the 3-D frustule shape and nanoscale features (pores, channels).

The amine-enriching surface functionalization protocol and electroless deposition process were then applied to *Coscinodiscus asteromphalus* diatom frustules and planar glass substrates. SE images of the starting *CA* frustules are shown in **Figure 2**a, c, and e. The *CA* frustule valves were nearly circular in shape with a diameter of ~100 μm. The *CA* frustule valves also possessed characteristic radial rows of holes with an average diameter of 1.2 ± 0.2 μm distributed in an approximately hexagonal local (quasi-periodic) arrangement, with an average center-to-center nearest neighbor hole distance of 2.3 ± 0.3 μm (where the ranges refer to ± one standard deviation about the average values). Each of the holes was surrounded by an uplifted rim on one side of the frustule (Figure 2e). SE

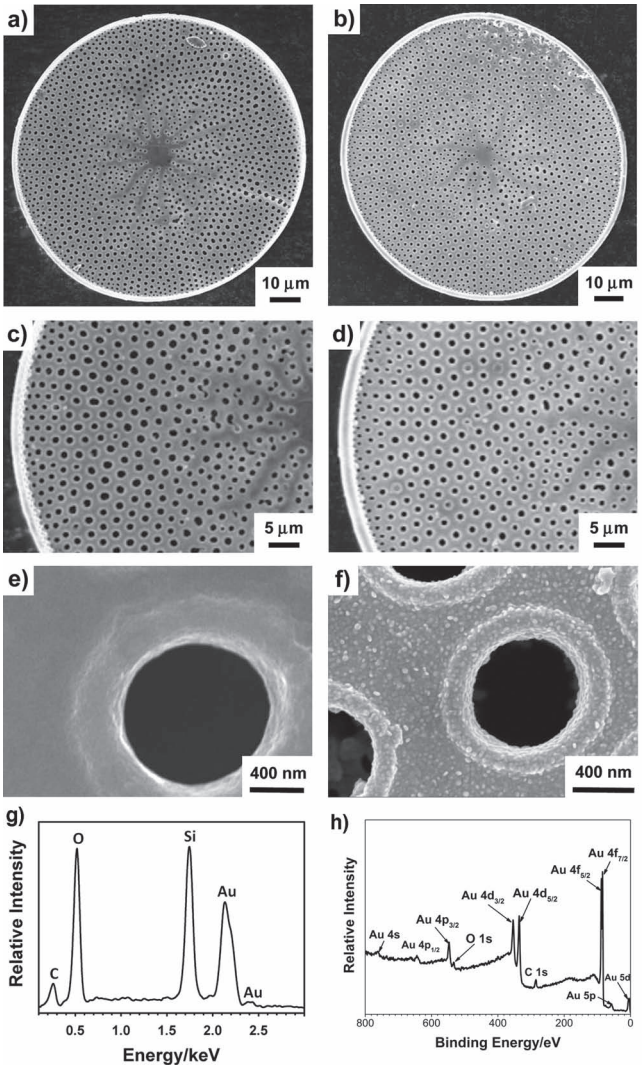

Figure 2. SE images of: a,c,e) A starting *C. asteromphalus* diatom frustule valve, and b,d,f) a gold-coated *C. asteromphalus* frustule valve. g) EDX and h) XPS analyses of such gold-coated frustules .

images of gold-coated *CA* frustules are shown in Figure 2b, d, and f. Comparison of the higher magnification SE images in Figure 2e and 2f confirmed the conformality of the coating; that is, although the coated surfaces exhibited a more granular, nanocrystalline appearance than for the starting frustules, gaps or cracks in the coating were not detected and the surface features of the *CA* valves (e.g., the uplifted rims surrounding the circular holes) were well preserved. EDX analysis (Figure 2g), X-ray photoelectron spectroscopic (XPS) analysis (Figure 2h), and X-ray diffraction (XRD) analysis (**Figure 3**a) confirmed the presence of appreciable elemental gold on the coated frustules. The XPS analysis revealed the presence of distinct peaks for gold but not for silicon, which indicated that the SiO_2 frustule surfaces were completely coated. Scherrer analysis of the gold diffraction peaks in Figure 3a yielded an average crystal size of 10.5 ± 0.2 nm. Analyses of SE images yielded a mean apparent gold nanoparticle size of ~22 ± 7 nm, which indicated that the

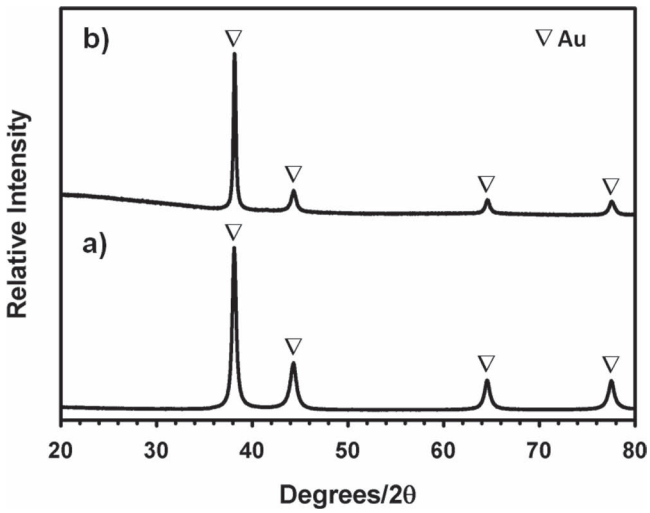

Figure 3. X-ray diffraction (XRD) analyses of: a) gold-coated *C. asteromphalus* diatom frustules and b) a gold-coated planar glass substrate.

gold nanoparticles were, on the average, comprised of about two nanocrystals. A gold coating was also generated on a planar glass substrate, using the same process as for the *CA* diatoms (**Figure 4**). The average thickness of the gold coating on this planar substrate was 84 ± 12 nm (i.e., comparable to the thickness of the gold coating applied to the *CA* diatom frustules, as discussed below). The presence and absence of peaks for gold and silicon, respectively, in the XPS analysis (Figure 4c) confirmed the complete nature of the coating on the planar glass substrate. Scherrer analysis of the XRD pattern obtained from this film (Figure 3b) and analyses of SE images of this coating yielded average gold crystallite and particle sizes of 14.6 ± 0.2 nm and 53 ± 20 nm, respectively. These values, like those for the *CA* diatom-derived gold structures, were substantially smaller than the values of the IR wavelengths used in subsequent optical analyses (i.e., such fine gold particles and crystals should result in minimal scattering of IR light).

Selective dissolution of the underlying silica from the gold-coated *CA* frustules yielded freestanding (hollow) gold structures that retained the overall 3-D morphology and fine features of the starting frustules. Top-down and cross-sectional SE images (the latter obtained via focused ion beam, FIB, milling) and EDX analysis of such gold structures are shown in **Figure 5**. The absence of detectable Si and O peaks in the EDX pattern (Figure 5f) confirmed the removal of the underlying silica template. The conformality and continuity of the gold coating enabled the freestanding gold structures to retain the overall 3-D frustule shape and finer features (such as the rims around the micron-sized holes, Figure 5c). FIB milled cross-sections of a freestanding gold structure (Figure 5d and e) revealed the hollow nature of these structures that resulted from complete removal of the silica template. The FIB cross-sections also revealed that the continuous gold coating possessed an average thickness of 95 ± 12 nm.

2.2. IR Transmission/Reflection Properties

Optical (transmission, reflection) images of a freestanding *CA*-derived gold structure, and the normalized infrared reflectance and transmission spectra obtained from this structure (after infiltration/coating with an index-matching oil), are shown in **Figure 6**. A reflection minimum (28%) and a transmission maximum (13%) were observed at wavelengths centered at ~4.1 μm and ~4.3 μm, respectively. Such IR reflection minima/transmission maxima were observed in multiple *CA*-derived freestanding gold structures but were not observed for the starting (uncoated) *CA* frustules or for planar gold-coated glass substrates (Figure 4d), which indicated that these spectral features were a result of both the frustule-derived structure and the gold chemistry.

The presence of such transmission maxima/reflection minima for the *CA*-derived gold structures indicated that the patterned array of subwavelength holes present on these structures were sufficiently ordered as to support the extraordinary transmission of light at wavelengths greater than the hole diameter (i.e., transmitted light of ~4.3 μm wavelength, holes of 1.2 μm average diameter). The transmission of light through metallic structures with patterned arrays of holes of subwavelength diameter, referred to as extraordinary optical transmission (EOT), has been reported for various metals and hole array patterns, including periodic,

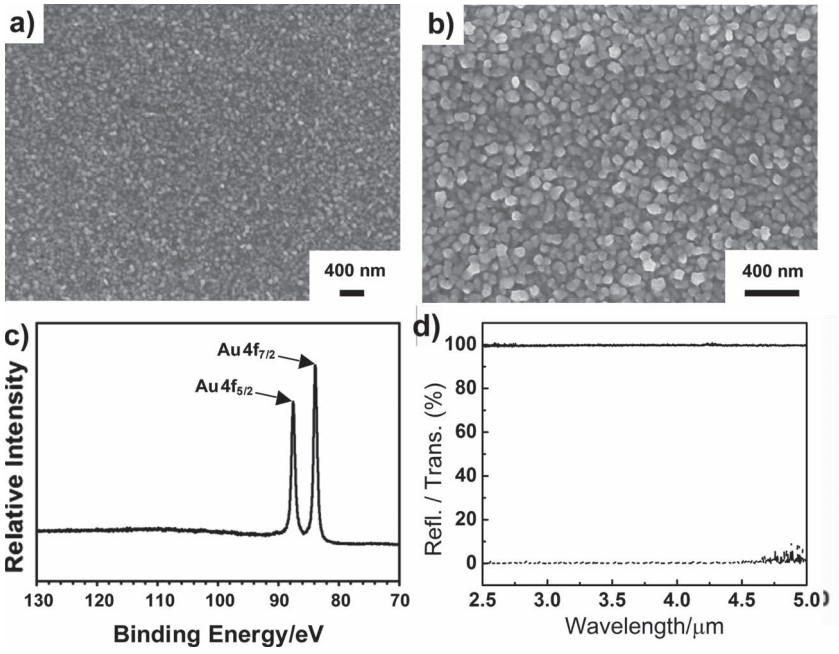

Figure 4. a, b) SE images and c) XPS analysis of a gold-coated planar glass substrate prepared in a similar manner as for the amine-amplified, gold-coated *C. asteromphalus* frustules. d) Reflectance (solid line) and transmittance (dashed) spectra of the planar gold-coated glass substrate, relative to an evaporatively deposited gold film.

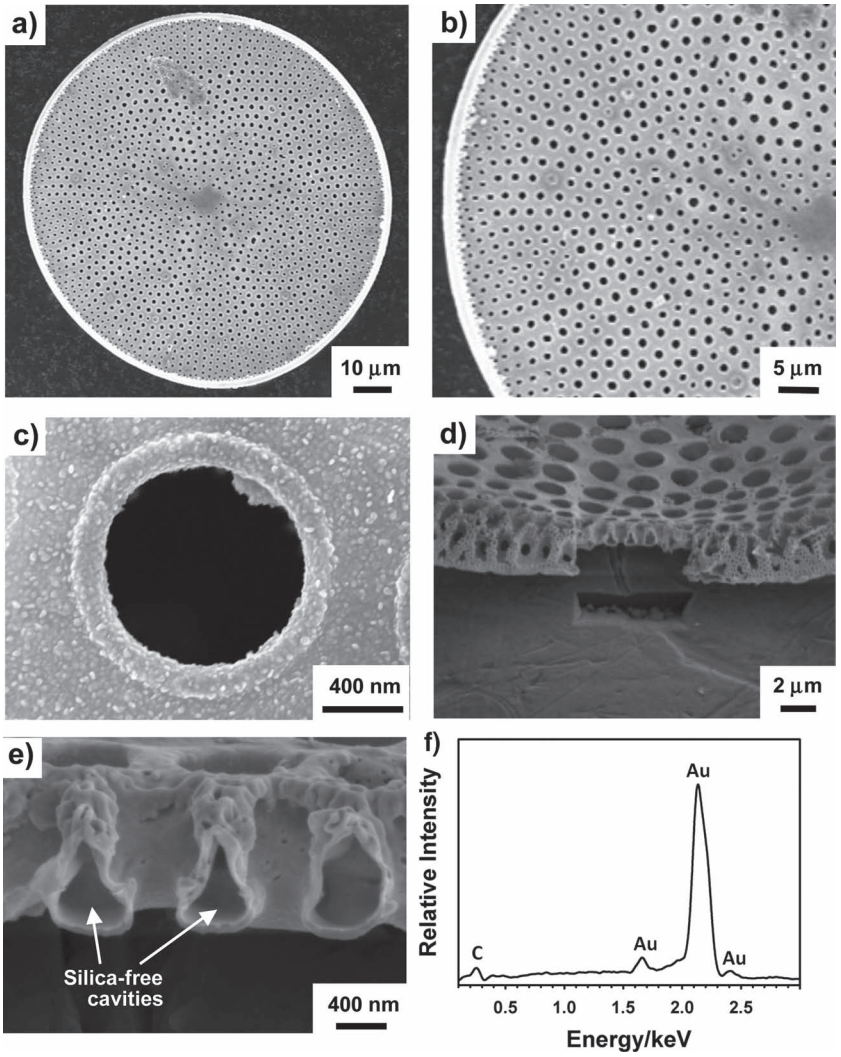

Figure 5. SE images of: a–c) a freestanding (silica-free) gold structure retaining the morphology of a *C. asteromphalus* diatom frustule valve, and d), e) ion-milled cross-sections of such a freestanding gold structure. f) EDX analysis of such a freestanding gold structure .

quasiperiodic, and aperiodic patterns.[10] However, the use of a self-replicating, biologically-derived 3-D template possessing arrays of subwavelength holes to generate such IR transmissive metallic structures has not been previously examined. To allow for comparison with the transmission results from the gold diatom replicas, planar gold films were prepared with hole patterns of the following types: i) a *CA* hole pattern (with the pore pattern observed in the replica in Figure 6), ii) a randomly perturbed *CA* hole pattern, iii) a periodic hexagonal hole pattern, and iv) a randomly perturbed hexagonal hole pattern. Each of these hole patterns was generated by FIB milling of continuous, conformal, and nanocrystalline planar gold films of the type shown in Figure 4a and b (prepared by the amine-enriching surface functionalization and electroless deposition process). SE images of the ion-milled gold films containing these patterned hole arrays are shown in **Figure 7**a–d.

The gold *CA* replica (Figures 6a and b), and the planar gold films with FIB-generated hexagonal and *CA* hole arrays (Figures 7a and c, respectively), exhibited the normalized transmission spectra shown in Figure 7e. All three types of gold structures exhibited a relatively strong long-wavelength transmission resonance, with the positions of these primary transmission peaks centered between 4.2 and 4.5 μm, although the planar gold films with the periodic hexagonal and quasi-periodic *CA* hole arrays exhibited stronger transmission resonances (51% at ~4.5 μm and 42% at ~4.2 μm, respectively) than did the gold replicas derived from *CA* diatoms (13% at ~4.3 μm). Interestingly, the Au *CA* replica, and the planar Au film containing the *CA* hole pattern, exhibited transmission maxima centered at nearly the same wavelength (~4.3 vs. ~4.2 μm, respectively).

In order to gain insight into the optical transmission properties of the gold *CA* replicas and the hole-patterned planar gold films, transmission spectra were calculated using a surface plasmon interference model reported by Pacifici, et. al.,[10d] that was tailored to the experimental optical geometry of the present work (i.e., for a ring of unpolarized light focused on the sample with angles of incidence varying from 14 to 30 degrees). This model treats the optical transmission through films with hole arrays as being due to the following fundamental processes: 1) optical excitation of surface plasmon polaritons (SPP) by scattering from individual holes, 2) propagation of SPPs to other holes in the array, which causes a phase shift ($k_{spp}a$, where k_{spp} is the SPP wavevector and a is the distance between holes) relative to the incident light at the neighboring holes (leading to interference between the SPP launched from neighboring holes and the incident field at a given hole), 3) transmission of the total field at each hole from the top through the hole, 4) launching and interference of SPPs from holes at the bottom surface, and 5) light emission by scattering of SPPs from holes on the bottom surface. This calculation yields the normalized (per hole) transmission for a given hole array pattern. In order to evaluate the impact of the periodicity of the hole arrays on infrared transmission through the gold structures, the calculated and experimental transmission spectra were further normalized by taking the ratio of the transmission of a given hole array to that of a randomly perturbed version of the same array. Such calculated normalized transmission spectra (per hole) are shown in **Figure 8**a (note: in this figure, normalized transmission values above or below unity refer to enhanced or suppressed transmission, respectively, relative to a film with a randomly perturbed version of the same type of hole array). For a planar gold film with 992 holes arranged in the same quasi-periodic pattern as for a *CA* gold replica (the replica shown in Figure 6), the calculated normalized spectrum exhibited enhanced transmission peaks centered at ~4.3 and ~3.2 μm,

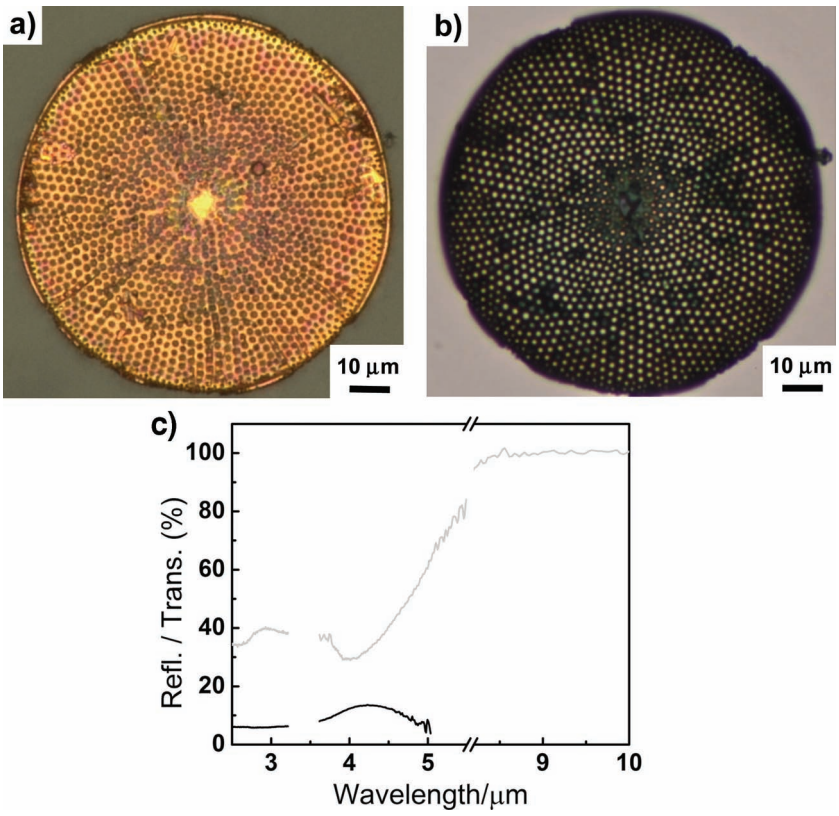

Figure 6. a) Reflection and b) transmission optical images of a *C. asteromphalus* frustule-derived freestanding (silica free) gold structure. c) Reflection (gray) and transmission (black) spectra of this freestanding gold structure (with the reflection and transmission data normalized relative to a planar gold film of the type shown in Figure 4 and an uncoated planar glass substrate, respectively). The freestanding *CA*-derived gold structure was placed on a glass slide, immersed in an index-matching oil, and capped with a cover slip. The planar gold reference film (on a glass slide) was covered with the index-matching oil and capped with a cover slip. The gap regions in the spectra in (c) coincide with C-H stretching absorption bands of the oil at 3.3–3.6 μm. Because the glass substrate became strongly absorbing at ~5 μm, the transmission spectrum was truncated at ≥ 5 μm .

and suppressed transmission valleys (minima) centered at ~3.4 and ~2.8 μm. This *CA*-based hole array possessed local hexagonal order (i.e., to within about 3–4 nearest hole neighbors) without extensive long-range periodicity. In light of such short-range order, a similar calculation was conducted for a planar gold film containing a perfectly-ordered hexagonal array with only 16 holes. The calculated transmission spectrum for this 16-hole periodic hexagonal array (also shown in Figure 8a) was found to be in reasonably good agreement with that calculated for the 992-hole quasi-periodic *CA* array. Such agreement indicated that the short-range order of holes in a *CA*-based array played a dominant role in enabling IR transmission through gold structures with such a quasi-periodic hole pattern.

The normalized transmission spectra calculated from the SPP interference-based model (Figure 8a) were then compared to the experimentally-measured normalized spectra shown in Figure 8b. Reasonably good agreement was observed between the calculated and experimentally-measured spectra at relatively long wavelengths; that is, for films possessing the periodic hexagonal and quasi-periodic *CA*-derived hole arrays, two transmission peaks (with the stronger primary peak detected at a longer wavelength) were observed at wavelengths greater than ~2.7 μm for both the calculated and measured spectra. For the film with the *CA*-derived quasi-periodic hole array, the strongest transmission peaks obtained from the calculated and experimentally-measured spectra were centered at ~4.3 μm (Figure 8a) and ~4.2 μm (Figure 8b), respectively. For the planar film with the periodic hexagonal hole array, the calculated and measured strongest transmission peaks were both centered at ~4.5 μm. Secondary transmission peaks in the calculated spectra were observed at ~3.2 μm and ~3.3 μm for the quasi-periodic *CA*-derived and periodic hexagonal hole arrays, respectively. For the measured spectra, such secondary transmission peaks also appeared to be located between 3.1-3.5 μm, although identification of the location of these measured secondary peaks was complicated by the presence of C-H absorption bands from the index-matching oil at 3.3–3.6 μm. A suppressed transmission valley observed in the calculated spectra for the quasi-periodic *CA*-derived hole array at ~3.4 μm also appeared to be present in the measured spectra for this array between 3.3 and 3.6 μm. A suppressed transmission valley observed in the calculated spectra for the periodic hexagonal hole array at ~3.6 μm was present in the measured spectra for this array at ~3.9 μm.

The SPP interference-based calculations predicted more intense transmission at 4.2–4.5 um than was measured for the gold *CA* frustule replicas. Structural features of the *CA* frustule replicas that may have influenced the extent of the measured transmission at these long wavelengths, and that were not considered in the model, include the curvature of the top and bottom surfaces of the gold replicas (seen in Figure 5d), the lateral variation in hole size (seen in Figure 5b), and the variation in hole size through the thickness of the *CA* frustule replica (seen in Figure 5e).

The location and intensity of the primary transmission resonance peaks for these patterned-hole gold structures were significantly influenced by the presence of the index-matching oil. When the oil was replaced with air, the transmission maximum shifted from a wavelength of ~4.3 μm to ~2.8 μm for the Au *CA* frustule replica. This change also resulted in a reduction in the peak transmission from 13% to 8.4%. Such shifts in peak transmission wavelength and changes in intensity were also observed for the planar gold films with periodic hexagonal hole arrays and quasi-periodic *CA*-derived hole arrays. These observations are consistent with the expected influence of the refractive indices of the media above and below the hole-patterned gold structures on the location of the transmission peaks associated with constructive interference of SPPs. For the oil-bearing specimens, the effective SPP index at the interface between the oil and the upper surface of the gold structure is increased,

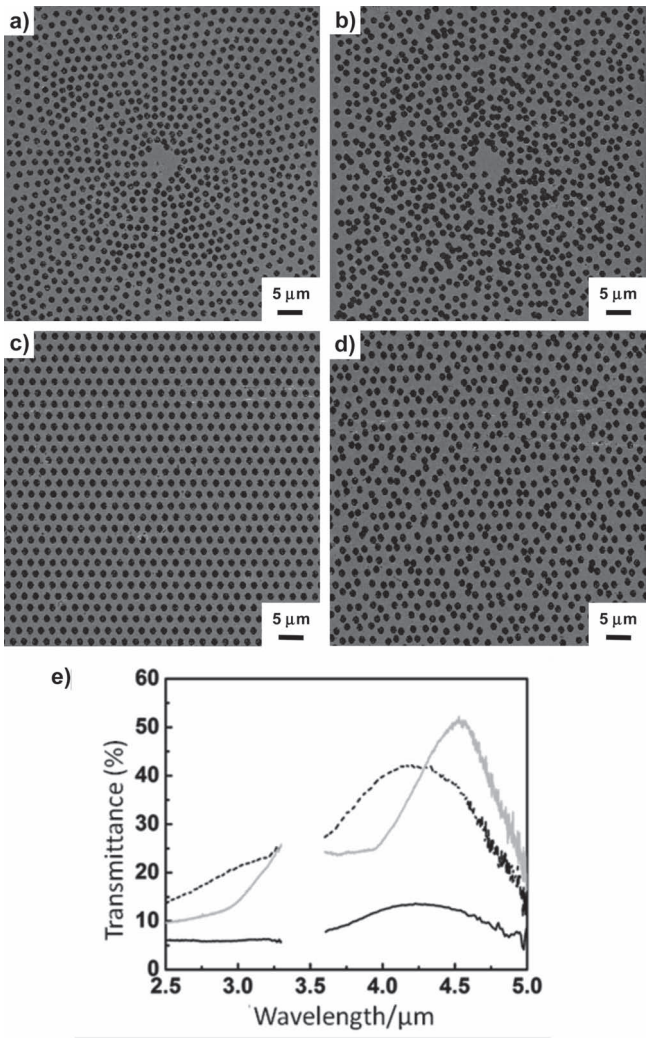

Figure 7. SEM images of planar gold films with various hole arrays fabricated by focused ion beam (FIB) milling: a) a hole pattern matching that of an actual quasi-periodic *CA* hole array (see Figure 6), b) a *CA* array pattern with random perturbations to hole positions, limited to the average spacing of the native hole array pattern, c) a periodic hexagonal hole array pattern with a hole spacing of 2320 nm, and d) a hexagonal hole array with random perturbations to hole positions. e) Transmission spectra obtained from a gold replica of a native *CA* diatom frustule (solid black), a planar gold film (as shown in a)) with a quasi-periodic hole array pattern obtained from a native *CA* diatom frustule (dashed black), and a planar gold film (as shown in c)) with a periodic hexagonal hole array pattern (gray).

leading to a larger effective SPP path length between holes and a shift of the transmission resonance to longer wavelength, as well as to better phase matching between the SPPs on the top and bottom giving an increase in transmission.

Since the first demonstration of EOT in metallic structures with sub-wavelength hole arrays,[12] numerous authors have examined the potential use of such structures for sensing, displays, imaging, communications, computing, lithography, and other applications.[13] However, no reports to our knowledge have been made of the use of self-replicating 3-D templates, such as diatom frustules, to generate freestanding structures exhibiting EOT. The coating-based process, and resulting diatom-derived gold replica structures, of the present work can provide attractive processing and morphological advantages as dispersible microparticles for EOT-based applications. For example, thin gold films (e.g., 100 nm thick) with nanopore array patterns, generated by electron beam lithography or focused ion beam milling, have been used as fast and sensitive EOT-based detectors of analytes in ambient or physiological fluids (e.g., detection of viruses, DNA, proteins, synthetic organic molecules via shifts in the EOT peak positions due to changes in the dielectric function at the metal surface).[13b–e] The present wet chemical coating-based process for fabricating microscale structures exhibiting EOT does not require the use of relatively expensive electron beam or ion beam (vacuum-based) techniques. Furthermore, the culturing of diatoms and the coating-based conversion process can both be readily scaled up to generate enormous numbers of freestanding 3-D metallic structures possessing similar (genetically-controlled) pore arrays. After appropriate functionalization to allow for selective binding to a particular analyte, large numbers of such gold microparticles may be dispersed in a fluid that may contain the analyte of interest. Owing to the robust nature of the gold frustule replicas, intense stirring of such structures in the fluid may be utilized for rapid transfer of the analyte to the gold surfaces (note: the *CA* frustule replicas of the present work survived stirring in aqueous solutions at 500 rpm for 12 h). The microparticles may then be optically interrogated *in situ* or quickly harvested via filtration for rapid optical analyses (note: the flat shapes of many diatom frustules, such as *C. asteromphalus*, allows for rapid alignment of the pore arrays on a flat substrate). The captured analyte may be detached from the diatom replica structures for further analyses. The large numbers of freestanding gold structures that may be generated with the present scalable process can provide a high total dispersable surface area for capturing a relatively large amount of analyte. The 3-D porous frustule replica morphology itself can also be attractive for sensing. For example, the long lengths of the pore channels of the gold *C. asteromphalus* frustule replicas of the present work (on the order of 1 μm), compared to the pore arrays in previously-reported planar EOT-based sensors prepared by electron beam or focused ion beam lithography (on the order of 100 nm[13b–e]), provide relatively large areas on the walls of the pore channels for the binding and sensitive detection of analytes. Frustules with a wide variety of quasi-periodic pore arrays (pore shapes, sizes, spacings, patterns) can be found among the extant 10^4–10^5 diatom species.[2] Diatom frustule replicas with particular pore patterns comprised of gold or other metals (i.e., Ag, Cu, Pd, Pt, Ni, and other metals that can be deposited via electroless deposition[14]) may be selected for EOT-based detection at particular wavelengths. Recent work has also shown that significant transparency may be induced in metallic films with disordered nanopore arrays by placing light-absorbing molecules in close proximity to the metal surfaces.[15] Hence, multiple frustule morphologies, metal compositions, and/or light-absorbing molecules may be utilized within a given batch of dispersible microparticles for the simultaneous harvesting and detection of multiple analytes in a particular fluid. The present scalable bio-enabled process provides a new and attractive capability for

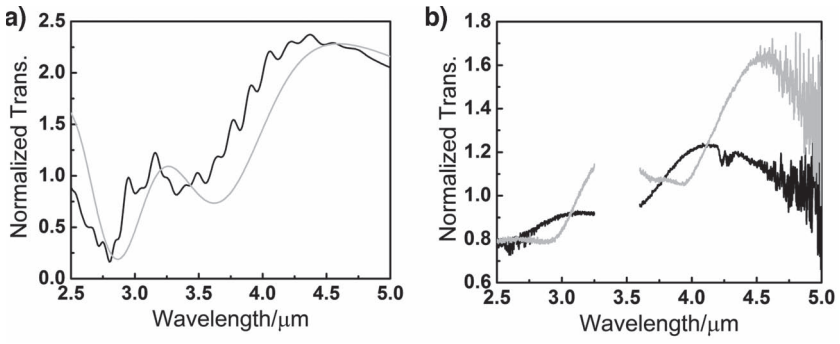

Figure 8. Normalized transmission spectra of hole-array structures fabricated in planar Au films using FIB milling. a) Calculated transmission efficiency spectra of gold films with a quasi-periodic *CA*-derived hole array pattern (black) and a periodic hexagonal array with 16 holes and a hole spacing of 2320 nm (gray). b) Experimental spectra obtained from planar gold films with a quasi-periodic *CA*-derived hole pattern normalized to a randomly perturbed *CA*-derived hole array pattern (black) and a periodic hexagonal hole array pattern normalized to a perturbed hexagonal hole array pattern (gray).

fabricating freestanding 3-D metallic structures for use as dispersible/harvestable microparticles for sensitive and tailorable EOT-based analyte detection.

In a more general sense, this work demonstrates that, by combining the attractive self-assembly characteristics of diatoms and other structure-forming organisms (i.e., massively-parallel, genetically-precise, direct 3-D assembly of structures with a wide selection of nano-to-microscale morphologies under ambient conditions) with a readily-scalable, highly-conformal, wet chemical conversion process, metallic assemblies with a variety of selectable 3-D morphologies may be mass produced in a sustainable manner. Proper selection of a 3-D shaped/patterned template from the extensive range of available biogenic morphologies, followed by shape-preserving conversion into an appropriate nanocrystalline element or alloy, can yield complex 3-D metallic structures with new (non-biological) properties for a host of applications.

3. Conclusions

Freestanding 3-D microscale nanocrystalline gold structures, with complex morphologies and fine patterned features inherited from silica diatom frustules, were synthesized via combined use of an amine-amplifying surface functionalization process and electroless gold deposition. By using a cyclic polyacrylate/polyamine protocol to significantly amplify the pendant amino groups attached to aminosilanized diatom frustule surfaces, a high density of gold (III) complexes could be bound to such surfaces and then reduced to generate a high population of heterogeneous gold nucleation sites for subsequent electroless gold deposition. Owing to the conformal and continuous nature of the resulting thin (<100 nm) nanocrystalline gold coatings, selective dissolution of the underlying silica template yielded freestanding gold structures that retained the 3-D shapes and fine patterned features of the starting frustules.

Freestanding diatom-derived gold structures with quasi-periodic hexagonal arrays of pores, inherited from *Coscinodiscus asteromphalus* diatom valves, exhibited transmission maxima and reflection minima at infrared wavelengths well above the average pore diameter. Such EOT was not observed for the starting silica diatom valves or for flat nonporous gold films, which indicated that such optical behavior resulted from the combined effects of the *CA* diatom-derived quasi-periodic hole structure and the gold chemistry. Enhanced transmission at similar infrared wavelengths was also observed for a planar gold film containing 992 holes arranged in a quasi-periodic pattern matching that of a *CA* diatom valve, as well as from a planar gold film with only 16 holes arranged in a perfectly periodic hexagonal array. The latter observation indicated that the quasi-periodic order of holes on the *CA*-derived gold replicas (i.e., with local hexagonal order that extended out to only about 3–4 nearest hole neighbors) played a dominant role in such extraordinary IR transmission. Calculations based on a surface-plasmon interference-mediated transmission model yielded wavelengths for such enhanced IR transmission that were in reasonable agreement with those obtained from experimental measurements of these patterned-hole gold structures.

The scalable wet chemical process described in this work (dendritic amplification of surface amines coupled with rapid, electroless metal deposition) provides an attractive capability for converting self-replicating 3-D templates possessing quasi-periodic pore arrays into freestanding metallic replica structures for EOT-based applications. This process may be extended to a variety of other self-replicating biogenic, or self-assembling synthetic, templates to yield 3-D micro/nanopatterned metallic structures for a range of optical, electrical, chemical, or structural applications.

4. Experimental Section

Diatom Culturing: A *Coscinodiscus asteromphalus* (*CA*) diatom strain (CCMP1814) was obtained from the Provasoli-Guillard National Center for Culture of Marine Phytoplankton (Bigelow Laboratory for Ocean Sciences, West Boothbay Harbor, ME, USA). The *C. asteromphalus* culture was grown in NEPC medium[8] at 18 °C under continuous illumination (~5700 ± 1100 lux) from cool white fluorescent bulbs for 3 weeks. The cultured diatom cells were harvested with the aid of a flow-through centrifuge operating at 18,180 g (Sorvall Evolution RC, Kendro Lab Products, Asheville, NC, USA). The resulting pellets containing a small amount of growth medium were then transferred to Falcon tubes (50 ml) and further centrifuged for 5 min at 4,500 g (5804R centrifuge, Eppendorf North America, Hauppauge, NY, USA). The pellets were then refluxed with nitric acid (8 M) at 100 °C for 1 h to remove organic material. The frustules were then washed repeatedly with de-ionized water until the natant water became neutral in pH. The frustules were then dried at 60 °C for >10 h.

Surface Amine Enrichment: Amine groups were introduced to the surfaces of *Aulacoseira sp.* and *C. asteromphalus* diatom frustules and glass slides (pre-cleaned micro slides, Catalogue No. 3010, Gold Seal Products, Portsmouth, NH, USA) via an aminosilanization treatment consisting of refluxing overnight in an aqueous solution comprised of 10 wt% of 3-[2-(2-aminoethylamino) ethylamino]propyl-trimethoxysilane (Sigma-Aldrich, St. Louis, MO, USA) and 3.5 wt% of concentrated

NH_4OH (30% solution of NH_3 in water, Fischer Scientific, Pittsburgh, PA, USA). The aminosilanized frustules and glass slides were then washed with de-ionized water, followed by washing with anhydrous ethanol. For some of the specimens, a dendritic polyacrylate/polyamine amplification treatment was used to amplify the amine groups on the template surfaces.[9] Aminosilanized specimens were first exposed to a solution (50 wt%) of dipentaerythritol penta-/hexa-acrylate (DPEPHA, Sigma-Aldrich) in ethanol on a rotator (30 rpm, Tube Rotator, VWR International, Suwanee, GA, USA) for 1 h at room temperature. This exposure was then followed by washing the specimens with anhydrous ethanol to remove unbound DPEPHA. The specimens were then exposed to a solution (50 wt%) of tris(2-aminoethyl)amine (TAEA, Sigma-Aldrich) in ethanol on the rotator (30 rpm) for 1 h at room temperature, followed by rinsing with anhydrous ethanol to remove unbound TAEA. The process of alternating exposure to a DPEPHA solution and TAEA solution was repeated four times (for a total of five cycles).

Electroless Gold Deposition and Selective Silica Dissolution: Amine-enriched diatom frustules and glass slides were incubated with a solution comprised of 5 wt% of chloroauric acid ($HAuCl_4$, Sigma-Aldrich) with 60 vol% of ethanol overnight at room temperature on the rotator (30 rpm). After rinsing four times with an ethanol solution (60 vol%), the diatom frustules and glass slides were incubated with a solution comprised of 0.16 M sodium borohydride ($NaBH_4$, Alfa Aesar, Ward Hill, MA, USA) with 60 vol% ethanol at room temperature at 300 rpm (Thermomixer R, Eppendorf North America) for 10 min. After rinsing four times with de-ionized water, the templates were immersed in a commercial electroless gold solution (Bright Electroless Gold, Transene Company, Inc., Danvers, MA, USA) that had been diluted by 50% in an aqueous solution of ethanol (60 vol%). A solution comprised of 0.16 M $NaBH_4$ with 60 vol% of ethanol was then introduced and the mixture was stirred for 3 min at 300 rpm (Thermomixer R) at room temperature. After rinsing four times with de-ionized water and once with anhydrous methanol, the gold-coated specimens were dried at 60 °C for >10 h. Selective dissolution of the underlying silica from the gold-coated frustules was conducted by immersing the coated frustules in a aqueous HF solution (5 wt%) overnight with shaking (500 rpm) at room temperature. The resulting freestanding gold structures were washed with DI water and then with anhydrous methanol, followed by drying in a 60 °C oven overnight.

Patterning of Pores in Flat Gold Films: A dual beam, focused ion beam (FIB) instrument (Nova Nanolab 200, FEI Company, Hillsboro, OR, USA) was used to obtain cross-sections of the freestanding diatom-derived gold structures and to generate pore patterns within planar gold films on glass slides. In the latter case, periodic and aperiodic pore patterns were imported into the FIB operating system to allow for the selective milling of such patterned pore arrays into the gold films. Such FIB patterning was conducted using a gallium ion energy of 30 KeV, a beam current of 0.1 nA, an incident angle of 0°, a dwell time of 100 µs, and a beam overlap of 50%.

Structural and Chemical Characterization :Scanning electron microscopy was conducted with a field emission scanning electron microscope (Leo 1530 FEG SEM, Carl Zeiss SMT Ltd., Cambridge, UK) equipped with an energy dispersive x-ray spectrometer (INCA EDS, Oxford Instruments, Bucks, UK). Cross-sections of the freestanding frustule-shaped metallic structures were obtained using the FIB instrument. X-ray diffraction analyses (X-Pert Pro Alpha 1 diffractometer, PANalytical, Almelo, The Netherlands) were conducted with Cu Kα radiation with an incident beam Johannsen monochromator and an Xcelerator linear detector. X-ray photoelectron spectroscopy (SSX-100, Surface Physics, Inc., Bend, OR, USA) was conducted at a base pressure of 3×10^{-7} Pa using an Al Kα source (1486.6 eV) and step sizes of 0.1 eV.

Optical Characterization: Suspensions of the freestanding diatom-derived gold structures in ethanol were injected onto a glass slide (Catalogue number 177399, Lab-Tek, Thermo Scientific, Portsmouth, NH, USA) and allowed to evaporate. Near- and mid-infrared reflectance and transmittance spectra of the freestanding gold replica structures on the glass slide were obtained using a Fourier-transform infrared spectrometer coupled to a microscope (FTS7000-UMA600, Agilent and Thermo Nicolet IN10MX mid-infrared microscope) that utilized a Cassegrain objective lens with a numerical aperture of 0.5 (giving inner and outer angles of the annular ring of light of 14 and 30 degrees, respectively). A variable aperture in the microscope was set to provide a field of view of 60 µm × 60 µm within a central region of the gold diatom replica structures. The reflectance spectra were normalized relative to an evaporatively-deposited gold mirror coating on a glass slide. Transmittance spectra of samples on a glass substrate in air were normalized relative to an uncoated glass slide. Transmittance and reflectance spectra were also measured for samples that had been infiltrated with, and coated on top by, an oil with a refractive index (Type A oil, refractive index = 1.5142 at 0.589 µm Cargille) matching that of the glass slide (1.523 at 0.589 µm), followed by capping with a cover slip (Gold Seal No. 0, Electron Microscopy Sciences, Hatfield, PA). Transmission spectra of the index-matched samples were normalized to an assembly comprising a glass slide, a 15 µm thick layer of index-matching oil (defined by a 15 µm thick spacer), and a cover slip.

Modelling of Optical Transmission: Transmission spectra were calculated using a surface plasmon interference model of the type reported by Pacifici et al.[10d,11] This model has been modified to match the experimental optical geometry of the present work, which involved a ring of unpolarized light focused on the sample with angles of incidence varying from 14 to 30 degrees. The effect of this non-normal incidence was accommodated by introducing a phase shift of the form to account for the difference in optical path length for light reaching pairs of holes:

$$\Delta\phi = \frac{2\pi}{\lambda} n(\lambda)\, a \sin\theta_i$$

where θ_i is the angle of incidence, λ is the free space optical wavelength, and $n(\lambda)$ is the wavelength-dependent refractive index of the index-matching oil. An amplitude factor was also included to account for the projection of the plane of polarization onto the surface of each hole array. The calculated transmission spectra were averaged over the range of incidence angles (14 to 30 degrees). Model parameters (plasmon coupling parameter, phase shift upon launch of SPP) were taken to be the same as in reference 10d. The dielectric function of our nanocrystalline Au film was found to be nearly identical to that reported by Palik.[11a] The dielectric function of the substrate was very similar to that of the index matching oil, so the oil dielectric function was used for the bounding medium on the top and bottom of the Au film.

Acknowledgements

This work was supported by the U.S. Air Force Office of Scientific Research via Awards No. FA9550-09-1-0162 (for FIB milling, XPS analyses, and electron microscopy), FA9550-09-1-0669 (for the syntheses of freestanding gold replicas of *C. asteromphalus* frustules), and FA9550-10-1-0555 (for the modeling and optical characterization of plasmon-mediated infrared transmission) and the U.S. Department of Energy, Office of Basic Energy Sciences, via Award No. DE-SC0002245 (for the surface functionalization/amine amplification of *Aulacoseira* diatom frustules). The authors acknowledge the Georgia Tech FIB2 Center established under NSF funding. The authors thank Prof. D. Pacifici of Brown Univ. for helpful discussions on the transmission modeling, Dr. Jianing Sun of Woollam, Inc. for measurement of the mid-IR dielectric function of our nanocrystalline gold films, and Mr. Craig Cameron for optical microscopy images of gold replicas of *CA* diatom frustules.

Received: November 10, 2011
Revised: December 13, 2011
Published online: March 21, 2012

[1] a) M. Srinivasarao, *Chem. Rev.* **1999**, *99*, 1935; b) J. R. Young, S. A. Davis, P. R. Bown, S. Mann, *J. Struct. Biol.* **1999**, *126*, 195; c) J. Alzenberg, A. Tkachenko, S. Weiner, L. Addadi, G. Hendler, *Nature* **2001**, *412*, 819; d) P. Vukusic, J. R. Sambles, *Nature* **2003**,

424, 852; e) J. C. Weaver, J. Aizenberg, G. E. Fantner, D. Kisailus, A. Woesz, P. Allen, K. Fields, M. J. Porter, F. W. Zok, P. K. Hansma, P. Fratzl, D. E. Morse, *J. Struct. Biol.* **2007**, *158*, 93; f) M. Cusack, A. Freer, *Chem. Rev.* **2008**, *108*, 4433.

[2] a) F. E Round, R. M. Crawford, D. G. Mann, *The Diatoms: Biology and Morphology of the Genera*, Cambridge University Press, New York, NY **1990**; b) D. G. Mann, S. J. M. Droop, *Hydrobiologia* **1996**, *336*, 19; c) R. Gordon, F. A. S. Sterrenburg, K. H. Sandhage, *J. Nanosci. Nanotechnol.* **2005**, *5*, 1–4; d) M. Hildebrand, *Chem. Rev.* **2008**, *108*, 4855; e) N. Kroger, N. Poulsen, *Ann. Rev. Gen.* **2008**, *42*, 83.

[3] K. H. Sandhage, R. L. Snyder, G. Ahmad, S. M. Allan, Y. Cai, M. B. Dickerson, C. S. Gaddis, M. S. Haluska, S. Shian, M. R. Weatherspoon, R. A. Rapp, R. R. Unocic, F. M. Zalar, Y. Zhang, M. Hildebrand, B. P. Palenik, *Int. J. Appl. Ceram. Technol.* **2005**, *2*, 317.

[4] a) K. H. Sandhage, M. B. Dickerson, P. M. Huseman, M. A. Caranna, J. D. Clifton, T. A. Bull, T. J. Heibel, W. R. Overton, M. E. A. Schoenwaelder, *Adv. Mater.* **2002**, *14*, 429; b) R. R. Unocic, F. M. Zalar, P. M. Sarosi, Y. Cai, K. H. Sandhage, *Chem. Comm.* **2004**, 795; c) Y. Cai, S. M. Allan, F. M. Zalar, K. H. Sandhage, *J. Am. Ceram. Soc.* **2005**, *88*, 2005; d) S. Shian, Y. Cai, M. R. Weatherspoon, S. M. Allan, K. H. Sandhage, *J. Am. Ceram. Soc.* **2006**, *89*, 694; e) Z. Bao, M. R. Weatherspoon, Y. Cai, S. Shian, P. D. Graham, S. M. Allan, G. Ahmad, M. B. Dickerson, B. C. Church, Z. Kang, C. J. Summers, H. W. Abernathy, III, M. Liu, K. H. Sandhage, *Nature* **2007**, *446*, 172.

[5] a) N. L. Rosi, C. S. Thaxton, C. A. Mirkin, *Angew. Chem. Int. Ed.* **2004**, *43*, 5500; b) C. S. Gaddis, K. H. Sandhage, *J. Mater. Res.* **2004**, *19*, 2541; c) E. K. Payne, N. L. Rosi, C. Xue, C. A. Mirkin, *Angew. Chem. Int. Ed.* **2005**, *44*, 5064; d) J. Zhao, C. S. Gaddis, Y. Cai, K. H. Sandhage, *J. Mater. Res.* **2005**, *20*, 282; e) D. Losic, G. Triani, P. J. Evans, A. Atancio, J. G. Mitchell, N. H. Voelcker, *Chem. Commun.* **2005**, 4905; f) S. M. Holmes, B. E. Graniel-Garcia, P. Foran, P. Hill, E. P. L. Roberts, B. H. Sakakini, J. M. Newton, *Chem. Commun.* **2006**, 2662; g) X. Cai, G. Zhu, W. Zhang, H. Zhao, C. Wang, S. Qiu, Y. Wei, *Eur. J. Inorg. Chem.* **2006**, 3641; h) U. Kusari, Z. Bao, Y. Cai, G. Ahmad, K. H. Sandhage, L. G. Sneddon, *Chem. Comm.* **2007**, 1177; i) Y. Fang, Q. Wu, M. B. Dickerson, Y. Cai, S. Shian, D. Berrigan, N. Poulsen, N. Kroger, K. H. Sandhage, *Chem. Mater.* **2009**, *21*, 5704; j) H. Zhou, T. Fan, X. Li, J. Ding, D. Zhang, X. Li, Y. Gao, *Eur. J. Inorg. Chem.* **2009**, 211; k) Y. Yu, J. Addai-Mensah, D. Losic, *Langmuir* **2010**, *26*, 14068.

[6] a) M. W. Anderson, S. M. Holmes, N. Hanif, C. S. Cundy, *Angew. Chem. Int. Ed.* **2000**, *39*, 2707; b) Y. Wang, Y. Tang, A. Dong, X. Wang, N. Ren, Z. Gao, *J. Mater. Chem.* **2002**, *12*, 1812; c) Y. Cai, K. H. Sandhage, *Phys. Stat. Sol. (a)* **2005**, *202*, R105; d) M. R. Weatherspoon, S. M. Allan, E. Hunt, Y. Cai, K. H. Sandhage, *Chem. Comm.* **2005**, 651; e) M. R. Weatherspoon, M. S. Haluska, Y. Cai, J. S. King, C. J. Summers, R. L. Snyder, K. H. Sandhage, *J. Electrochem. Soc.* **2006**, *153*, H34; f) Y. Cai, M. B. Dickerson, M. S. Haluska, Z. Kang, C. J. Summers, K. H. Sandhage, *J. Am. Ceram. Soc.* **2007**, *90*, 1304; g) E. M. Ernst, B. C. Church, C. S. Gaddis, R. L. Snyder, K. H. Sandhage, *J. Mater. Res.* **2007**, *22*, 1121; h) Z. Bao, E. M. Ernst, S. Yoo, K. H. Sandhage, *Adv. Mater.* **2009**, *21*, 474.

[7] J. Noyes, M. Sumper, P. Vukusic, *J. Mater. Res.* **2008**, *23*, 3229; b) L. De Stefano, I. Rea, I. Rendina, M. De Stefano, L. Moretti, *Opt. Express* **2007**, *15*, 18082; c) E. De Tommasi, I. Rea, V. Mocella, L. Moretti, M. De Stefano, I. Rendina, L. De Stefano, *Opt. Express* **2009**, *18*, 12203; d) T. Fuhrmann, S. Landwehr, M. El Rharbi-Kucki, M. Sumper, *Appl. Phys. B* **2004**, *78*, 257; e) S. Yamanaka, R. Yano, H. Usami, N. Hayashida, M. Ohguchi, H. Takeda, K. Yoshino, *J. Appl. Phys.* **2008**, *103*, 074701.

[8] http://www.botany.ubc.ca/cccm/NEPCC/esaw.html (accessed March, 2012).

[9] a) M. R. Weatherspoon, M. B. Dickerson, G. Wang, Y. Cai, S. Shian, S. C. Jones, S. R. Marder, K. H. Sandhage, *Angew. Chem. Int. Ed.* **2007**, *46*, 5724; b) G. Wang, Y. Fang, P. Kim, A. Hayek, M. R. Weatherspoon, J. W. Perry, K. H. Sandhage, S. R. Marder, S. C. Jones, *Adv. Funct. Mater.* **2009**, *19*, 2768.

[10] a) H. F. Ghaemi, T. Thio, D. E. Grupp, T. W. Ebbesen, H. J. Lezec, *Phys. Rev. B* **1998**, *58*, 6779; b) Q.-J. Wang, J.-Q. Li, C.-P. Huang, C. Zhang, Y.-Y. Zhu, *Appl. Phys. Lett.* **2005**, *87*, 091105; c) J. Xue, B.-Q. Dong, X. Wang, R. Yang, Z.-C. Xu, Y. Chen, E. Huq, W. Zeng, X.-P. Qu, R. Liu, *Microelectron. Eng.* **2010**, *87*, 1340; d) D. Pacifici, H. J. Lezec, L. A. Sweatlock, R. J. Walters, H. A. Atwater, *Opt. Express* **2008**, *16*, 9222.

[11] a) E. D. Palik, *Handbook of Optical Constants of Solids*, Academic Press, Orlando, FL, **1985**; b) M. Rubin, *Solar Energy Mater.* **1985**, *12*, 275.

[12] T. W. Ebbesen, H. J. Lezec, H. F. Ghaemi, T. Thio, P. A. Wolff, *Nature* **1998**, *391*, 667.

[13] a) C. Genet, T. W. Ebbesen, *Nature* **2007**, *445*, 39; b) M. J. Levene, J. Korlach, S. W. Turner, M. Foquet, H. G. Craighead, W. W. Webb, *Science* **2003**, *299*, 682; c) A. A. Yanik, M. Huang, O. Kamohara, A. Artar, T. W. Geisbert, J. H. Connor, H. Altug, *Nano Lett.* **2010**, *10*, 4962; d) R. Gordon, D. Sinton, K. L. Kvanagh, A. G. Brolo, *Acc. Chem. Res.* **2008**, *41*, 1049; e) A. Lesuffleur, H. Im, N. C. Lindquist, S.-H. Oh, *Appl. Phys. Lett.* **2007**, *90*, 243110; f) C. Liu, V. Kamaev, Z. V. Vardeny, *Appl. Phys. Lett.* **2005**, *86*, 143501; g) E. Laux, C. Genet, T. Skauli, T. W. Ebbesen, *Nat. Photonics* **2008**, *2*, 161; h) H. J. Lezec, A. Degiron, E. Devauz, R. A. Linke, L. Martin-Moreno, F. J. Garcia-Vidal, T. W. Ebbesen, *Science* **2002**, *297*, 820; i) W. Srituravanich, N. Fang, C. Sun, Q. Luo, X. Zhang, *Nano Lett.* **2004**, *4*, 1085.

[14] a) B. Durkin, C. Steinecker, *Kirk-Othmer Encyclopedia of Chemical Technology*, 5th Edition, Vol. *9* (Ed. A. Seidel), Wiley & Sons, New York **2005**, 685; b) Y. S. Chen, A. Tal, D. B. Torrance, S. M. Kuebler, *Adv. Funct. Mater.* **2006**, *16*, 1739; c) P. C. Hidber, W. Helbig, E. Kim, G. M. Whitesides, *Langmuir* **1996**, *12*, 1375; d) R. A. Farrer, C. N. LaFratta, L. Li, J. Praino, M. J. Naughton, B. E. A. Saleh, M. C. Teich, J. T. Fourkas, *J. Am. Chem. Soc.* **2006**, *128*, 1796.

[15] J. A. Hutchison, D. M. O'Carroll, T. Schwartz, C. Genet, T. W. Ebbesen, *Angew. Chem. Int. Ed.* **2011**, *50*, 2085.